The Length of the Shortest Telomere as the Major Determinant of the Onset of Replicative Senescence

Zhou Xu,* Khanh Dao Duc,† David Holcman,† and Maria Teresa Teixeira*,[1]

*Laboratoire de Biologie Moléculaire et Cellulaire des Eucaryotes, Institut de Biologie Physico-Chimique, Centre National de la Recherche Scientifique, Université Pierre et Marie Curie, FRE3354, 75005 Paris, France, †Institute for Biology (IBENS), Group of Computational Biology and Applied Mathematics, École Normale Supérieure de Paris, 75005 Paris, France

ABSTRACT The absence of telomerase in many eukaryotes leads to the gradual shortening of telomeres, causing replicative senescence. In humans, this proliferation barrier constitutes a tumor suppressor mechanism and may be involved in cellular aging. Yet the heterogeneity of the senescence phenotype has hindered the understanding of its onset. Here we investigated the regulation of telomere length and its control of senescence heterogeneity. Because the length of the shortest telomeres can potentially regulate cell fate, we focus on their dynamics in *Saccharomyces cerevisiae*. We developed a stochastic model of telomere dynamics built on the protein-counting model, where an increasing number of protein-bound telomeric repeats shift telomeres into a nonextendable state by telomerase. Using numerical simulations, we found that the length of the shortest telomere is well separated from the length of the others, suggesting a prominent role in triggering senescence. We evaluated this possibility using classical genetic analyses of tetrads, combined with a quantitative and sensitive assay for senescence. In contrast to mitosis of telomerase-negative cells, which produces two cells with identical senescence onset, meiosis is able to segregate a determinant of senescence onset among the telomerase-negative spores. The frequency of such segregation is in accordance with this determinant being the length of the shortest telomere. Taken together, our results substantiate the length of the shortest telomere as being the key genetic marker determining senescence onset in *S. cerevisiae*.

TELOMERES constitute essential nucleoprotein structures at the ends of chromosomes. In eukaryotes, they are composed of a variable number of short TG-rich tandem repeats running from the 5′- to 3′-ends, often protruding in a 3′-overhang and coated with specialized proteins. Telomeric repeats are specified by the RNA moiety of a cellular reverse transcriptase, telomerase, that synthesizes *de novo* telomeric sequences for their maintenance (Cech 2004; Blackburn and Collins 2011). In the absence of this enzyme, the progressive shortening of telomeres ultimately leads to a cell-cycle arrest, a pathway called senescence. One major function of telomeres is to prevent the cellular machinery from recognizing the chromosome ends as accidental DNA breaks (Jain and Cooper 2010). Indeed, disruption of telomeric structures leads to chromosome fusions and genomic instability. Despite this essential conserved function, telomeres display a striking variability in their length, the dynamics of which is not well understood. Furthermore, while telomere shortening is observed in the absence of telomerase, how telomere length determines senescence remains elusive.

Senescence was first described in human fibroblasts cultured *ex vivo* as a proliferative limit for cells, despite their being metabolically viable (Hayflick 1965). While other types of stimuli can similarly limit proliferation, telomere attrition is one of the best characterized stimuli and may contribute to aging in some human tissues (Campisi and D'adda Di Fagagna 2007; Jeyapalan and Sedivy 2008). Importantly, this mechanism has been considered one of the most potent barriers to cancer cell proliferation in the early stages of tumorigenesis. In *Saccharomyces cerevisiae*, in the absence of telomerase, the set of 300- to 350-bp-long telomeres shortens at a rate of 3–4 bp per cell division while cells progressively lose their viability (Lundblad and Szostak 1989; Marcand *et al.* 1999; Wellinger and Zakian 2012). This cell-cycle arrest is modulated by Tel1 and dependent on Mec1, the yeast orthologs of the mammalian checkpoints ataxia telangiectasia mutated (ATM) and ataxia telangiectasia-

doi: 10.1534/genetics.113.152322
Manuscript received April 18, 2013; accepted for publication May 23, 2013
Available freely online through the author-supported open access option.
Supporting information is available online at http://www.genetics.org/lookup/suppl/doi:10.1534/genetics.113.152322/-/DC1.
[1]Corresponding author: Institut de Biologie Physico-Chimique (IBPC), CNRS, FRE3354, 13, rue Pierre et Marie Curie, 75015 Paris, France. E-mail: teresa.teixeira@ibpc.fr

and Rad3-related (ATR) phosphatidylinositol 3-kinases (Ritchie *et al.* 1999; Enomoto *et al.* 2002; Ijpma and Greider 2003). Since their activation is also involved in mammalian senescence (D'adda Di Fagagna *et al.* 2003), this suggests a conservation of the early steps of the cellular response to short telomeres. The current model is that as telomeres shorten, they lose components that prevent them from being recognized as an accidental DNA break and subsequently activate ATM/ATR pathways (D'adda Di Fagagna *et al.* 2003).

One striking characteristic of replicative senescence is its intrinsic heterogeneity. Intraclonal and interclonal variations have been observed in the proliferative potential of human fibroblasts as well as in yeast (Smith and Whitney 1980; Lundblad and Szostak 1989; Ritchie *et al.* 1999), suggesting that stochastic processes may be at play. For instance, telomeres could themselves acquire, in a progressive and stochastic manner, a senescence-signaling state as they shorten (Blackburn 2000). Along this line, the length of the shortest telomeres, rather than the mean telomere length, would dictate cell fate. Short telomeres were shown to trigger senescence in mammals (Hemann *et al.* 2001; Zou *et al.* 2004; Armanios *et al.* 2009) and we previously demonstrated in *S. cerevisiae* that introducing a single very short telomere accelerated senescence in a telomerase-negative context and triggered senescence signaling, *e.g.*, the recruitment of both Tel1 and Mec1 (Abdallah *et al.* 2009). However, the appreciation of the relevance of this finding has been limited by the lack of information on the distribution of native telomere lengths in wild-type *S. cerevisiae* cells. On the other hand, in mammalian cells, mitochondrial dysfunction may also affect telomere-dependent senescence, and conversely telomeric signals may induce mitochondrial failure (Passos *et al.* 2007; Sahin *et al.* 2011). More generally, this perspective points to a complex picture where metabolic and DNA damage (including telomere attrition) pathways interact to induce senescence (Sahin and Depinho 2012). Thus, to assess the relative contribution of short telomeres to senescence and their interference with other pathways, knowledge on the telomere length distribution within a cell emerges as an indispensable step.

In *S. cerevisiae* and mammals, shorter telomeres have a higher probability of being elongated by telomerase than longer ones (Hemann *et al.* 2001; Teixeira *et al.* 2004; Britt-Compton *et al.* 2009). A protein-counting mechanism has been proposed to explain this telomere length regulation (Lustig *et al.* 1990; Marcand *et al.* 1997; Van Steensel and De Lange 1997). In *S. cerevisiae*, this mechanism rests on the coating of telomeric repeats by the protein Rap1, which, through its interaction with the *R*ap1-*i*nteracting *f*actors Rif1 and Rif2, inhibits its telomerase elongation (Hardy *et al.* 1992; Marcand *et al.* 1997; Wotton and Shore 1997). Telomerase inhibition depends on the number of these factors, which in turn depends on telomere length. Then, elongation of shortened telomeres by telomerase holoenzyme involves a telomeric protein, Cdc13, and part of the machinery of DNA damage response (Wellinger and Zakian 2012). The number of Rap1/Rif1/Rif2 would therefore create a telomere-length-dependent negative feedback loop for the recruitment and/or activity of telomerase, theoretically maintaining telomere length distribution within controlled bounds. It is not clear, however, whether this mechanism is sufficient to account for the homeostasis of telomere length and to explain the dynamics of telomere length distribution.

Here, we studied the dynamics of telomere length by integrating the underlying protein-counting mechanism into a stochastic model. The model predicts a skewed distribution for telomere length that we experimentally validated by measuring the length of identified single telomeres. The distribution predicts a significant gap between the shortest telomere and the others. To test the significance of this gap in senescence, we compared senescence onsets of pairs of telomerase-negative cell lineages separated by either a mitosis or meiosis event. We found that meiosis segregates a major determinant of senescence onset, while mitosis leads to an identical senescence phenotype in the two cell lineages. Therefore, we propose that the length of the shortest telomere in the cell, rather than telomere-independent stochastic events, determines replicative senescence onset in *S. cerevisiae*.

Materials and Methods

A full version of this section can be found in the Supporting Information.

Materials

Infrared fluorescent oligonucleotide probes, with either DY682 or DY782 fluorophores at the 5′- and 3′-ends, were synthesized by and purchased from Eurofins MWG Operon. Chemicals were from Sigma-Aldrich, unless stated otherwise. *Nde*I, *Bst*EII, and *Bst*NI enzymes were purchased from New England Biolabs.

Yeast strains

The yT337 diploid strain, used throughout this study, was built by crossing haploid cells of W303 background: *Mat***a**/α, *ura3-1/ura3-1*, *trp1-1/trp1-1*, *leu2-3,112/leu2-3,112*, *his3-11,15/his3-11,15*, *can1-100/can1-100*, *ADE2/ADE2*, *TLC1/tlc1*::*Pr*α*Nat*. Haploid cells were generated by the sporulation of yT337, and the genotype of the spores was systematically tested by PCR amplifying a sequence in either the endogenous *TLC1* gene or the *Pr*α*Nat* marker.

Single-telomere Southern blot

yT337 diploid cells were sporulated on a potassium acetate medium and tetrads were dissected on a Singer MSM system 400 device. Spores were allowed to grow for 24 hr (~12 population doublings or PD) and were inoculated in 50 ml liquid culture. After 24 hr of exponential growth (~16 PD), cells were collected. Genomic DNA was extracted and purified using a Qiagen DNA kit and genomic tips 20/G, following the manufacturer's instructions. Then 4 μg genomic DNA was digested either with *Bst*NI or sequentially with *Nde*I and *Bst*EII restriction enzymes. Digested products were ethanol precipitated, resuspended in loading buffer (10 mM

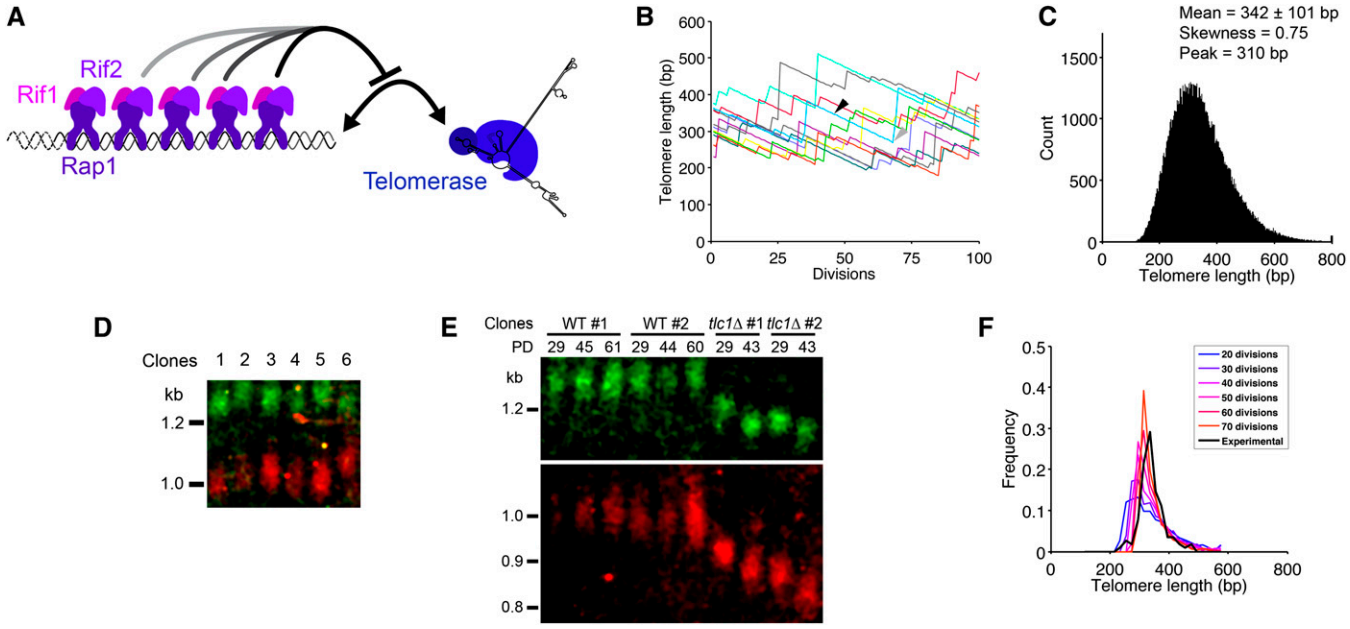

Figure 1 Telomere length distribution by simulation and single-telomere Southern blot. (A) The protein-counting mechanism is based on the measurement of telomere length by Rap1/Rif1/Rif2 binding to telomeric repeats and an inhibition of telomerase elongation depending on the number/concentration of these complexes. (B) Trajectories of 10 independent telomeres over 100 divisions. Depending on the length, a telomere (blue trajectory) can shorten by length *a* over several consecutive divisions (solid arrowhead) and then be elongated by a random length *b* (shaded arrowhead). (C) Telomere length distribution at equilibrium. Equation 1 was iterated 500 times starting with 100,000 telomeres drawn from an uniform distribution between 200 and 400 bp, and the resulting telomere length distribution was plotted (bin size, 3 bp). (D) Representative single-telomere Southern blot. Six independent *TLC1* wild-type spores derived from *TLC1/tlc1*Δ heterozygous diploids were grown for 24 hr on YPD plates and then transferred to liquid culture for another 24 hr at exponential growth (for a total of ∼30 population doublings). The Southern blot was performed on *Nde*I- and *Bst*EII-digested genomic DNA using simultaneously oT355 (green) and oT360 (red) fluorescent probes, designed to detect I-L and VI-R telomeres, respectively. (E) Single-telomere Southern blot with oT355 and oT360 fluorescent probes performed on telomerase-positive (wild type, WT) or negative (*tlc1*Δ) cells. *TLC1/tlc1*Δ diploid cells were sporulated, and the four spores from a tetrad were grown for 24 hr on a plate and then in liquid YPD medium for the total indicated population doublings (PD). (F) Comparison of experimental and simulated data of telomere length distribution. Plot of 117 experimental measurements of telomere length from single-telomere Southern blot as in D (black line, bin size, 20 bp) and 1000 simulated values $\overline{L}_i \in [|1:1000|]$ (colored lines, bin size, 20 bp) for 20, 30, . . ., 70 divisions. The latter were obtained as follows: after drawing randomly 100 initial lengths L_i^0 from the theoretical distribution in C, we applied the dynamics of Equation 1 to 1000 telomeres with initial length L_i^0 to get, after 50 divisions, a mean length $\overline{L}_i$. This was done for each plot, corresponding to 20, 30,. . ., or 70 divisions (blue to orange lines).

Tris pH 8.0, 1 mM EDTA, 5% glycerol, 0.04% xylene cyanol FF), and run in a 1.2% agarose gel for 14 hr at 60 V. The gel was then soaked in a denaturation bath (0.4 M NaOH, 1 M NaCl) for 30 min and transferred by capillarity on a Biodyne B charged nylon membrane (Pall). Hybridization of the membrane followed Rapid-hyb buffer protocol (Amersham). Briefly, the membrane was prehybridized at 52° in Rapid-hyb buffer for 1 hr. Fluorescent oligonucleotide probes (30 pmol) (Supporting Information, Table S1) were then added and allowed to incubate for 1 hr. Extensive washes were consecutively performed with 2× SSC, 0.5% SDS (at 52° for 10 min); 2× SSC, 0.1% SDS (at 37° for 20 min); and 0.1× SSC, 0.1% SDS (at room temperature for 30 min). Infrared (682-nm and 782-nm) fluorescence was read in an Odyssey Fc LI-COR apparatus, with a 10-min exposure time for each fluorescence wavelength.

Quantitative senescence assay

The quantitative senescence assay used in this study is a modified version of the semiquantitative senescence assay described in Abdallah *et al.* (2009), detailed in File S1.

Results

Mathematical model of telomere length dynamics and prediction of telomere lengths

The comprehensive understanding of the impact of short telomeres on the onset of senescence in *S. cerevisiae* has been hampered by the lack of knowledge of the actual telomere length distribution within cells. We therefore modeled the distribution of telomere lengths using the current knowledge on the regulation of telomere length homeostasis. We modeled the length of a single telomere after n divisions. In *S. cerevisiae*, the opposing effects of constitutive shortening and elongation by the telomerase holoenzyme regulate telomere length (Figure 1A). Thus, in our model, a telomere of length L_n is shortened by length a (shortening rate) at each cell division and then can either be elongated by telomerase by length b (number of nucleotides added by telomerase), with a probability $P(L_n)$, which depends on the telomere length, or not be elongated with probability $1 - P(L_n)$. Thus, the dynamics for L_{n+1} is

$$L_{n+1} = \begin{cases} L_n - a, & \text{w.p. } 1 - P(L_n) \\ L_n - a + b, & \text{w.p. } P(L_n) \end{cases}, \qquad (1)$$

where a is obtained from the empirical mean shortening rate of ~3–4 bp (Lundblad and Szostak 1989; Singer and Gottschling 1994; Nugent *et al.* 1996; Marcand *et al.* 1999) (w.p., *with probability*). Because telomerase processivity does not correlate with telomere length (Teixeira *et al.* 2004), we considered that the elongation length b is a random variable, independent of the telomere length L_n, and its probability follows a geometrical law ($\Pr\{b = k\} = p(1 - p)^k$) of parameter p. The parameter p was obtained by fitting the cumulative distribution function of empirical elongation lengths (Teixeira *et al.* 2004) (see File S1 and Figure S1, B and C). To approximate the probability $P(L_n)$, we used the empirical elongation frequency obtained for various telomere lengths (Teixeira *et al.* 2004), which is valid for telomeres longer than ~100 bp, as in telomerase-positive cells. We fitted it with the function

$$P(L_n) = \begin{cases} \dfrac{1}{1 + \beta(L_n - L_0)} & \text{if } L_n \geq L_0 \\ 1 & \text{otherwise,} \end{cases} \qquad (2)$$

where β and L_0 are fitting constant parameters (Table 1 and Figure S1A). Expression 2 was inferred from the biochemical process described in Figure 1A and in File S1. Since the probability $P(L_n)$ is fitted to experimental data, it accounts for any coupling between telomeres. For instance, it captures the possibility that a change of length of some telomeres affects the length of a single one due to a competition for a common resource, *e.g.*, telomerase.

We used Equation 1 to simulate a population of independent telomere lengths. To visualize the behavior of these telomeres over time, we plotted the dynamics of 10 independent telomeres (Figure 1B). Each telomere can undergo successive rounds of shortening (solid arrowhead in Figure 1B) and then be elongated by a random length b (shaded arrowhead in Figure 1B). The choice between shortening and elongation is controlled by the probability $P(L_n)$ (see Equations 1 and 2). We simulated 100,000 independent such telomeres starting with a uniform initial distribution and found that the overall distribution converges to a steady state (Figure 1C), with the following characteristics: mean $\pm$SD = 342 $\pm$ 101 bp, skewness = 0.75, and peak around 310 bp.

Experimental validation of the theoretical telomere length distribution

To validate the distribution obtained from our numerical simulations, we measured the length of single telomeres in wild-type (telomerase-positive) haploid yeast clonal culture by single-telomere Southern blot. For this purpose, we identified restriction sites (corresponding to *Nde*I, *Bst*EII, and *Bst*NI enzymes) that cut close to the telomeric repeats (<1.5 kb) and designed specific fluorescent-labeled oligonucleotide probes for a set of identified and unique telomeres, mostly X-element-only ones (see File S1 and Table S1). For any single telomere, differences in length were observed among independent clones, as shown in Figure 1D for the VI-R and the I-L telomeres. We also note that there was no obvious correlation between two different telomeres in their respective interclonal length variations, indicating independent length regulation among telomeres (Figure 1D, for instance, compare VI-R and I-L telomere signals for clones 4, 5, and 6). To further confirm that the signals corresponded to telomeres, we also performed the analysis on *tlc1*Δ cells, which lack the essential RNA component of telomerase (Singer and Gottschling 1994), and observed a smear that decreased in size with increased population doublings (Figure 1E and Figure S2). The mean shortening rate we measured was 3.2 bp per generation, consistent with others' results (Lundblad and Szostak 1989; Singer and Gottschling 1994; Nugent *et al.* 1996; Marcand *et al.* 1999).

We plotted the telomere length distribution of all the single telomere measurements of telomerase-positive cells and the resulting mean plus or minus the standard deviation was 341 $\pm$ 41 bp, with skewness = 0.73, and peak around 325 bp (Figure 1F). The distribution was more peaked than the simulated one (Figure 1C). Indeed, as we needed a sufficient amount of DNA starting with a single cell (48 hr), each initial telomere went through ~30 rounds of replication. Because the mean length of each telomere in the cell population converges toward the equilibrium length during this period, the distribution of the telomere length measurements in this experiment setting is expected to be more concentrated than the initial distribution. To compare this experimental distribution with the analytical one, we randomly picked telomere lengths from the simulated distribution (Figure 1C). Each of these lengths was used as initial condition for the next step: we simulated 1000 trajectories with the stochastic model and averaged them to reproduce telomere length change induced by cell growth in liquid culture. Figure 1F shows the distributions after 20, 30, ..., 70 divisions compared with the experimental data. There was no statistical difference between the simulations of 20, 30, and 40 divisions and the experimental data (χ^2 goodness-of-fit test, P = 0.17, 0.066, and 0.14, respectively). After 50, 60, and 70 divisions, however, the experimental and numerical distributions diverge (χ^2 goodness-of-fit test, P = 0.054, 0.054, and 0.012, respectively).

Table 1 Parameters of the model

Parameter	Estimated value, based on (reference)
p	0.026 (Teixeira *et al.* 2004)
β	0.045 (Teixeira *et al.* 2004)
L_0	90 (Teixeira *et al.* 2004)
a	3 or 4 with probability 0.5 (Lundblad and Szostak 1989; Marcand *et al.* 1999)

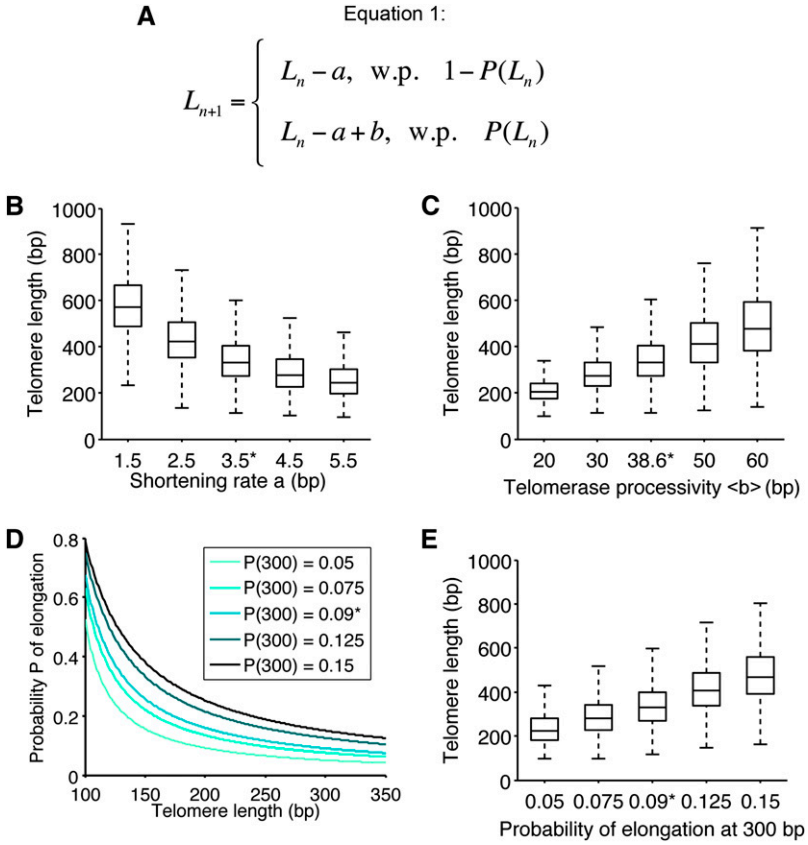

Figure 2 Impact of the model parameters on telomere length distribution. (A) Equation 1 describes the stochastic behavior of a telomere at each cell division: it can either shorten by the shortening rate *a* with a length-dependent probability $1 - P(L_n)$ or shorten and then be elongated by the length *b*, which is telomerase processivity, with probability $P(L_n)$. (B) Influence of the shortening rate on telomere length distribution. The distribution was simulated as in Figure 1C, for different values of the mean shortening rate *a* (see Equation 1), with 10,000 simulations. Control value of 3.5 bp is indicated by *. Boxes represent the interquartile range (25th–75th percentiles, median indicated by horizontal line) of the distribution, and whiskers extend to the 5th and 95th percentiles. (C) Influence of telomerase processivity on telomere length distribution. We proceeded as in B, but for different values of $\langle b \rangle$ (see Equation 1 in A), the number of nucleotides added per elongation (telomerase processivity). Control value of 38.6 bp indicated by *. (D) The probability of elongation was plotted as a function of the telomere length for different values of the ratio $\beta = k_1/k_2$, which reflects the biochemical equilibrium between elongation and shortening of telomeres (see Equations 3 and 4 in File S1). These values defined a range of probabilities of elongation by telomerase at 300 bp from 0.05 to 0.15. Control distribution of Figure 1C for value $P(300) = 0.09$, inferred from data in Teixeira *et al.* (2004), is indicated by *. (E) Influence of the probability of elongation on telomere length distribution. We proceeded as in B, but for different values of the parameter $\beta = k_1/k_2$ chosen as in D. Telomere length distributions are shown as a function of the probability of elongation at 300 bp.

Therefore, our simulated distribution was in good agreement with the experimental distribution of telomeres in a single cell (Figure 1, C and F). We thus consistently found the distribution of telomere lengths by both modeling and experimental measurements of single telomeres.

Sensitivity of the model to variations in the parameters

To evaluate the impact of various parameters of the model, we first compared the steady-state distributions of telomere length by iterating Equation 1 (Figure 2A) 500 times on 10,000 independent telomeres using different values for the shortening rate a, the mean of telomerase processivity $\langle b \rangle$, and the elongation probability parameter β (Figure 2). We observed that both the mean and the standard deviation of the telomere length distribution were highly sensitive to the shortening rate a (Figure 2B). We also found an increased positive skewness with increasing shortening rates, which correlated with a decreased and stabilized mean length. In our model, a shortening rate of ~3–4 bp per division would be consistent with the experimentally determined mean telomere length and with the experimental distribution in general.

We then assessed the contribution of telomerase processivity (Figure 2C). The mean length of telomere distribution was linearly correlated with telomerase processivity and no change in skewness could be observed, indicating that telomerase processivity has a role only in setting the mean telomere length and does not contribute to the asymmetry of the distribution.

To study the effect of different elongation probabilities, we changed the parameter β, which expresses the equilibrium between telomere extendable and nonextendable states (see File S1). Our simulations showed that this value had to be tightly controlled (around the measured value from data in Teixeira *et al.* 2004) if the mean length of telomeres was to be maintained, as slight variations strongly affected the distribution and the mean (Figure 2, D and E, compare distributions for $P = 0.075$, $P = 0.09$, $P = 0.125$).

Interestingly, the mean of the distribution can be computed for the parameters of the model: the mean shortening rate $\langle a \rangle$, the mean processivity $\langle b \rangle = (1-p)/p$, and the parameter β. We obtain from Equation 1 the mean equilibrium length $L_{eq} = L_0 + \frac{1}{\beta}([1-p]/<a>p-1)$. This expression confirms the linear behavior of L_{eq} as a function of $1/\langle a \rangle$.

While telomere distribution was quantitatively sensitive to the variations of parameters (Figure 2), the simulations always converged and resulted in biologically relevant distributions (for instance, the mean length was always in the range 200–550 bp), highlighting the robustness of the model.

The dynamics of telomere length results from the protein-counting mechanism

We studied the dynamics of telomere length by simulation and compared it to data from (Marcand *et al.* 1999), where the elongation of a short telomere or the shortening of a long one was measured over many population doublings. First we

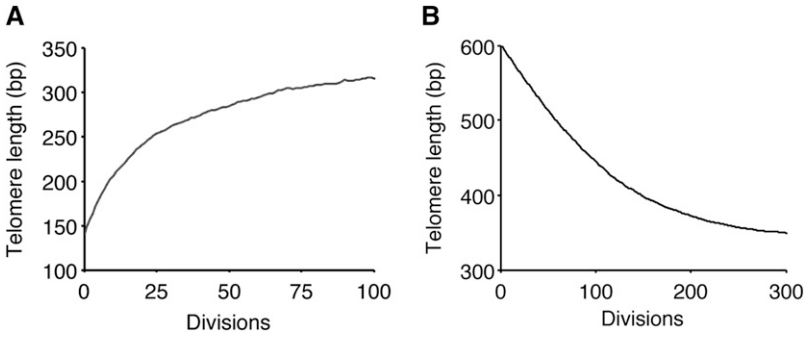

Figure 3 Simulation of telomere length dynamics. (A) Starting with an initial length of 140 bp, the dynamics of a short telomere return to steady-state length was simulated. The plot shown is an average over 10,000 simulations. (B) Dynamics of the shortening of a long telomere in the presence of telomerase. Same procedure as in A, starting from an initial length of 600 bp.

set a telomere at 140 bp and ran simulations until generation 100 in the presence of telomerase. By averaging this procedure over 10,000 runs, we found that the telomere length increased and converged exponentially to the mean of the stationary distribution (= 342 bp) (Figure 3A), with a rate of convergence $\mu = 0.89$ (Figure 3A). This linear convergence is in good agreement with the experimental linear dynamics observed previously (with an empirical rate $\mu = 0.926$, Marcand *et al.* 1999). Then we studied the dynamics of a long telomere returning to a normal length. In another set of numerical simulations, we let a long telomere of 600 bp evolve in the presence of telomerase and analyzed the average of 10,000 runs (Figure 3B). Strikingly, we reproduced the characteristic two-phase profile of the plot in Marcand *et al.* (1999), with a linear decrease in the first phase and a "fine-tuning" phase as the length was closer to the wild-type length. We calculated the initial shortening rate in the first phase and found a value of 2.1 bp per generation, as compared to 2.1–2.3 bp per generation measured in the presence of telomerase (Marcand *et al.* 1999). Interestingly, these values are lower than the shortening rate in the absence of telomerase (~3–4 bp per generation), both experimentally and by simulations. In our model, this is explained by the fact that elongation by telomerase occurs even for long telomeres, albeit at a low frequency (0.004–0.007), which contributes to an effective lower shortening rate. Therefore, the model closely reproduced the experimental dynamics of telomeres.

How short is the shortest telomere?

Because the shortest telomeres could potentially initiate senescence signaling, we investigated their dynamics in the presence of telomerase. From the stationary distribution of telomere length, we drew 32 values for the 32 telomeres and repeated it 10,000 times. The numerical simulations revealed that the mean lengths of the four shortest telomeres were, respectively, 180 ± 24, 202 ± 21, 217 ± 20, and 229 ± 20 bp (Figure 4A). The shortest telomere was on average 22 bp shorter than the second one and 162 bp shorter than the mean over all telomeres. In another simulation, we focused on the dynamics of the shortest telomeres in the presence of telomerase by tracking the length of the four shortest telomeres over time (Figure 4B). We observed that the length of the shortest telomere varied considerably compared to that of the others. The gap between the shortest telomere and the others was the most prominent, even though it was not observed at all time points. Considering that in the absence of telomerase, telomeres shorten at a global constant rate, we expect that this gap will be maintained in most cells during replicative senescence. Hence, the length of the shortest telomere is expected to be set in each cell during the last cell division before telomerase removal and to vary considerably from cell to cell.

We thus showed that the shortest telomere is well separated from the other telomeres, with a significant variance that may lead to a heterogeneity in triggering senescence.

Mitosis in the absence of telomerase produces two cell lineages with similar senescence

We then explored the possibility that a specific telomere, possibly the shortest, causes the senescence onset heterogeneity found in telomerase-negative independent clones. Variations in senescence onset in sister *TLC1*-deficient spores derived through sporulation from *TLC1/tlc1Δ* diploids have been described before (Ritchie *et al.* 1999). This indicated that a senescence onset determinant is segregated during meiosis. This determinant could be the set of telomeres that are differentially segregated among the spores in meiosis (Walmsley and Petes 1985). Therefore, we first tested whether cells possessing a similar set of telomeres would behave similarly during senescence. We compared senescence kinetics in pairs of cells derived from a mitosis event after telomerase removal (mother and daughter cells) (Figure 5A). We let a *tlc1*Δ spore divide once, separated the two cells by microdissection, and analyzed their respective senescence. To detect subtle differences in senescence rates, we optimized a spot assay we had developed previously (Abdallah *et al.* 2009) (Figure 5A). As shown for a representative pair in Figure 5A, mitosis did not generate differential senescence in the resulting mother and daughter cell lineages. This result was reproduced in eight independent experiments and there was no statistical difference at any passage between mother and daughter cell lineages ($P > 0.1$ for all pairs at any passage, Student's unpaired *t*-test). From this experiment, we inferred that (i) the spot assay was not sensitive enough to discriminate slight differences in senescence that could result from telomere length differences generated during a mitotic event, supposedly a 3′-overhang

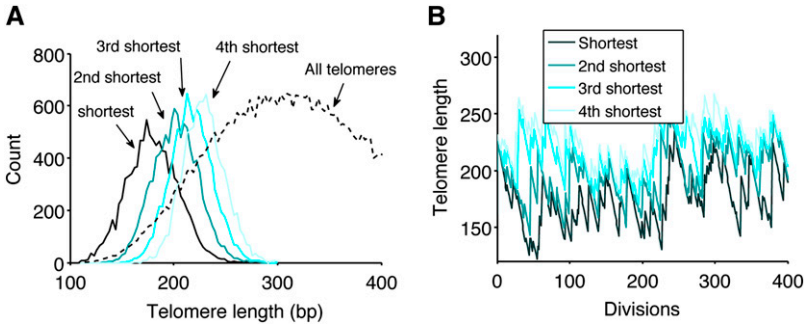

Figure 4 Distribution of the shortest telomeres in the presence of telomerase. (A) From the stationary distribution in Figure 1C, 32 lengths were randomly drawn. This draw was repeated 10,000 times, and the distribution of the four shortest telomeres was plotted (bin size, 3 bp). The distribution of all telomeres from Figure 1C is reproduced as a dotted line for comparison. (B) Representative dynamics of the four shortest telomeres in a given cell over 400 divisions. The lengths of 32 telomeres were simulated and the four shortest ones were tracked over time.

length difference (~10 nt), and that (ii) if telomere-independent events affecting senescence rates did occur, then they did so at similar frequencies in the mother and daughter cell lines.

Meiosis segregates a determinant of senescence

We then studied replicative senescence heterogeneity among *tlc1Δ* sister spores derived from a *TLC1/tlc1Δ* diploid using our assay to rate senescence. Quantitative analysis of 35 tetrads was performed and two types of tetrads were found, as illustrated in Figure 5B: one for which the two *tlc1*Δ spores displayed similar senescence onsets (Figure 5B, right) and one for which they had different senescence onsets (Figure 5B, left). The latter type represented 71% of tetrads (Figure 6), since significant differences in the senescence index of the two *tlc1Δ* sister spores were found in 25 out of the 35 tetrads ($P < 0.05$ at the second or third passage, Student's *t*-test). This demonstrated that, in contrast to mitosis, meiosis segregates a determinant of senescence onset. Since our diploid is a homozygote except for the telomerase RNA gene locus, we hypothesized that this determinant stems from the telomere set, which is different in each of the four spores of the tetrads. Other possibilities include imprinting or other epigenetic phenomena.

The shortest telomere as the major determinant of senescence onset

We reasoned that the ratio of tetrads in which the two *tlc1*Δ spores display different senescence to the total number of tetrads is indicative of how senescence onset is controlled: this ratio should vary with distinct hypotheses. We explored the simple hypothesis that the length of a specific telomere, probably the shortest telomere, segregated during meiosis, is a dominant "allele" setting the onset of senescence and estimated the theoretical segregation of this telomere using classical tetrad analysis.

While the following reasoning works equally for any specific telomere, we apply it to the shortest telomere, which is arguably the best candidate for being the signaling telomere. In the *TLC1/tlc1Δ* diploid, at prophase I, there are 128 telomeres that have just replicated. If we first neglect the difference in length of the two sister chromatid telomeres (see below), we can consider 64 telomere lengths (each corresponding to two sister chromatid telomeres). These 128 telomeres segregate between the four spores with one major rule: that sister chromatid telomeres cannot fall into the same spore. Because the distance centromere–telomere is the largest in a chromosome arm, meiotic recombination systematically shuffles telomeres between homologous chromosomes, resulting in telomeres randomly distributed among the four spores. We then analyzed how telomeres differentially fall into the two *tlc1Δ* sister spores, taking into account that the *TLC1* locus is genetically independent from telomeres (see File S2, for more details). If the shortest telomere controls senescence onset, then calculations point out that the shortest telomere in each of the two *tlc1Δ* spores resulting from meiosis is different in length in ~80% of the tetrads (Figure 6; see File S2 for more details). If this hypothesis does not hold true, a minimal postulate would be that senescent cells cannot distinguish between the shortest and the second shortest telomeres. In this scenario, the ratio of tetrads in which different senescence between the two *tlc1Δ* spores is observed to the total number of tetrads should drop down to ~46% (Figure 6). Other hypotheses would result in even lower ratios. For instance, if the mean telomere length determined senescence onset, then all tetrads would display the same senescence for their two *tlc1Δ* spores (0% of different senescence for the two *tlc1Δ* spores). This is, however, not the case.

Two phenomena are expected to modulate the calculated ratios. First, it is not known if telomerase acts after the premeiotic semiconservative DNA replication and, if so, if it acts in only one of the two sister chromatids. If it does, then the 80% ratio should slightly increase (we estimated this increase at ~2%; see File S2). Second, differences in senescence that are below the sensitivity of the assay are not accounted for, resulting in any experimental value being an underestimation of the ratio.

The 71% ratio we experimentally obtained was significantly different from the 46% ratio (χ^2 goodness-of-fit test, $P = 0.0025$) and could not be statistically distinguished from the 80% ratio (χ^2 goodness-of-fit test, $P > 0.2$) (Figure 6). Therefore, we concluded that (i) the length difference between the shortest and the second shortest telomeres predicted from simulations was frequently large enough for the spot assay to detect differences between the resulting senescence onsets and that (ii) our results were consistent with the shortest telomere controlling senescence as a dominant allele.

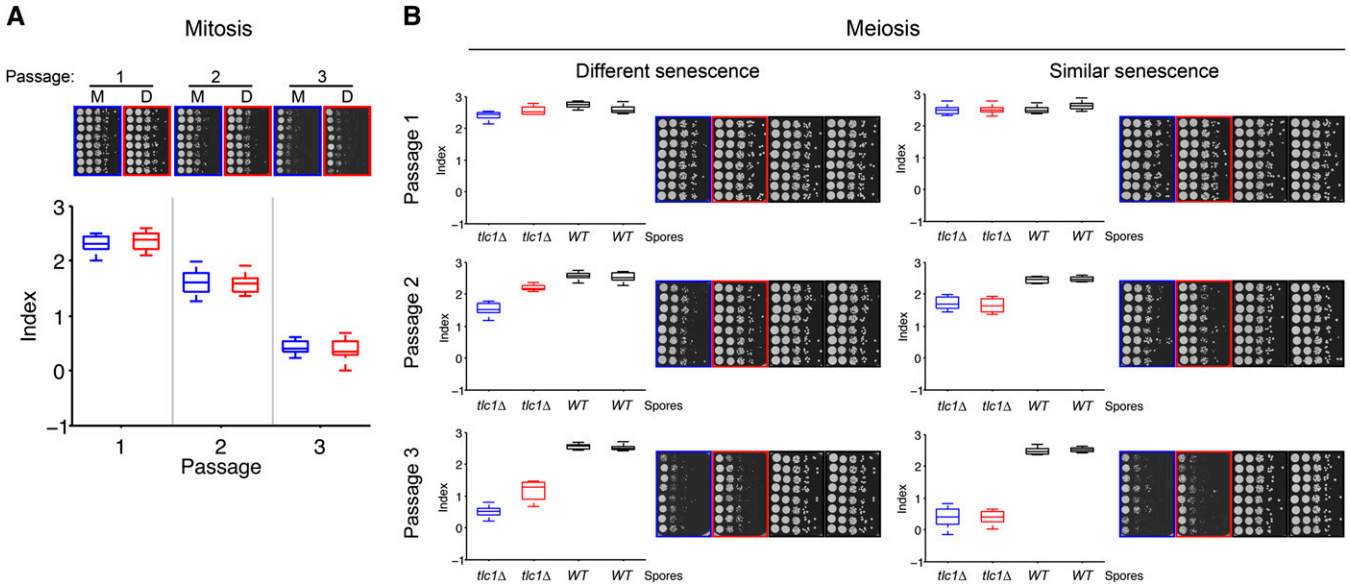

Figure 5 Meiosis, in contrast to mitosis, segregates a senescence determinant. (A) After sporulation, *TLC1*/*tlc1*Δ tetrads were dissected and *tlc1*Δ spores were allowed to undergo one division. The mother and daughter cells were then separated by microdissection and grown for 2 days on a rich medium agar plate. Each resulting colony was then spotted in eight replicates with 10-fold dilutions and grown for 2 days. Each replicate was individually passaged two more times. One representative spot assay of a pair of mother (bordered in blue, M) and daughter (bordered in red, D) cells is shown. Bottom: senescence indices are represented as boxplots (see File S1). Overall, $n = 8$ independent experiments. (B) Representative examples of spot assays for differential or similar senescence onsets for the two *tlc1*Δ spores of a tetrad. In each case, both the boxplot representation of the senescence index and the raw pictures of the spot assays for three passages are shown. The two *tlc1*Δ spores are depicted in blue and red, *TLC1* spores are in black. Overall, $n = 35$ tetrads were analyzed.

Discussion

This study investigates the relationship between telomere length regulation, telomere length distribution, and senescence onset. We combined mathematical modeling and numerical simulations with experimental data to address this issue in *S. cerevisiae*. We accounted for the molecular regulation of telomere length using a model that reveals the stochastic dynamics of telomere length. The predicted length distribution of the shortest telomere, together with genetic evidence on the segregation of a senescence determinant in meiosis, highlights a key role for the shortest telomere in governing senescence initiation.

A stochastic study of telomere length distribution and dynamics

Previous mathematical models on telomeres focused on how telomeres shorten in mammalian cells within a telomerase-deficient cell population and provided significant insights into the role of capping states and external stress conditions, the molecular dynamics of telomere shortening, and the variability of senescence onset (Levy *et al.* 1992; Kowald 1997; Tan 1999; Proctor and Kirkwood 2002; Proctor and Kirkwood 2003; Op Den Buijs *et al.* 2004; Arkus 2005; Rodriguez-Brenes and Peskin 2010). In addition, one of these studies built on the t-loop structure as the molecular basis of its model, a structure that has been observed in many eukaryotic telomeres (Griffith *et al.* 1999; Rodriguez-Brenes and Peskin 2010) but not in *S. cerevisiae*. This study gave novel insights into telomere length regulation dynamics in the presence of telomerase and could fit experimental telomere length distribution in senescence.

Here, we based our stochastic model on well-established molecular mechanisms underlying telomere length homeostasis in the presence of telomerase in *S. cerevisiae*. The stochastic Equation 1 accounts for two sources of fluctuations. First is the choice, at each division, to increase or not the telomere length with a probability $P(L_n)$. Second, once this choice is made, the length of elongation b is also a random variable, which follows a geometrical law. We could predict the steady-state distribution for telomere length. The asymmetry of the distribution, as revealed by the positive skewness, is indicative of the preferential elongation of short telomeres by telomerase. Indeed, the sharper slope on the left of the distribution, corresponding to shorter telomeres, results from the high probability of their "rescue."

We experimentally confirmed the distribution we simulated by measuring the lengths of many single telomeres. While telomere length distribution is experimentally documented in humans thanks to Q-FISH experiments that allow for the measurement of single native telomeres (Martens *et al.* 2000; Canela *et al.* 2007), to our knowledge there are no such studies in budding yeast because of technical issues. We thus developed and optimized a single-telomere Southern blot to provide direct data on telomere length distribution.

Our model was also consistent with data on telomere dynamics published in Marcand *et al.* (1999), where they

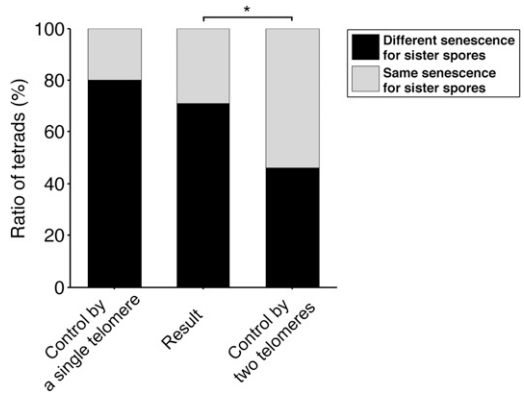

Figure 6 Experimental and theoretical ratios of tetrads in which sister telomerase-negative spores display different/similar senescence. "Control by a single telomere" refers to hypothesis 1 of File S2. "Control by two telomeres" to hypothesis 2 and "Result" is the experimental ratio obtained from meiosis segregation experiments as shown in Figure 5B. * indicates a statistical difference ($P = 0.0025$) using Pearson's χ^2 goodness-of-fit test.

analyzed how a single short or long telomere returns to a wild-type length in the presence of telomerase. Moreover our simulations showed a significant contribution of elongation events in buffering the shortening of a long telomere in the presence of telomerase. Our modeling approach was thus able to predict telomere length distribution and reveal a biological impact of telomerase in the elongation of long telomeres.

The protein-counting mechanism is the major mechanism of telomere length homeostasis

We could directly predict a relevant distribution and dynamics of telomere length from the protein-counting mechanism. This mechanism and the stochastic model we derived basically depend on (i) an inhibitory molecule whose local concentration is linearly correlated to telomere length (*e.g.*, Rap1/Rif1/Rif2) and (ii) a biochemical competition reaction for the same substrate (*e.g.*, the telomere) between this molecule and another (*e.g.*, telomerase), leading either to shortening or elongation of a telomere. As a consequence, our model should also be valid with other organisms where the protein-counting model operates, despite a different telomeric architecture. For instance, the numerical values we used for the parameters in Equations 1 and 2 stem from experimental data that do not make assumptions about the actual proteins acting at the telomeres.

The parameter analysis of telomere length distribution predicts how a specific regulator mutant can affect telomere length distribution. With more available experimental data, it would be insightful to clarify the role of regulators such as Pif1 (Schulz and Zakian 1994) or Tbf1 (Brevet *et al.* 2003) in the distribution of telomere length using the present analysis. Overall, our results strongly support the protein-counting mechanism as the major mechanism of telomere length homeostasis in *S. cerevisiae*.

A specific telomere, likely the shortest, controls senescence in S. cerevisiae

In our simulations, the mean length of the shortest telomere is ~80 bp longer than the ~100-bp-long critically short telomere described in Abdallah *et al.* (2009). This length (~100 bp) allows the corresponding strain to grow for ~45 generations in the absence of telomerase until senescence, compared to 60–80 generations for wild-type cells lacking telomerase. While these values are far from being precise, given the heterogeneity of senescence onset, they give a difference of ~15–35 generations between the two conditions, which is consistent with the difference of their shortest telomere length leading to $(180–100)/3.5 \approx 23$ generations (assuming a constant shortening rate of 3.5 bp per generation) of difference in the senescence onset. The simulations therefore support a potential role for the shortest telomere in signaling senescence. Moreover, its standard deviation is larger than that of the others: the shortest telomere is thus more prone to variations from cell to cell. We tested the hypothesis that this could explain interclonal variations of senescence onset in telomerase-deficient cells (Lundblad and Szostak 1989; Ritchie *et al.* 1999).

In mammalian cells, heterogeneity in senescence is accounted for by complex mechanisms with intricate relationships such as telomere shortening and/or uncapping, DNA damage, mitochondrial failure, or accumulation of reactive oxygen species (Smith and Whitney 1980; Passos *et al.* 2007; Sahin and Depinho 2012). If this is also the case in *S. cerevisiae*, we should observe random variations in senescence even though the initial set of telomeres is given. We thus analyzed the senescence of mother and daughter cell lineages after a mitosis event, since the mother and daughter cells have a similar set of telomeres. Interestingly, we did not find any difference in their senescence onset with our assay. We conclude that in *S. cerevisiae*, while there may be stochastic modulations of senescence similar to mammalian cells, their effect is either constant or weak compared to the fate forced on the cell lineage by telomere attrition. Senescence onset in budding yeast is thus tightly genetically determined in the initial single cell without telomerase and not driven by strong stochastic processes.

We then analyzed senescence in cells with "shuffled" telomeres, taking advantage of meiosis. In contrast to mitosis, meiosis segregated a determinant of senescence in a certain number of tetrads (71%) but not in others. Considering telomeres as alleles, we predicted different values for the ratio of tetrads with differential senescence in the two telomerase-negative spores to the total number of tetrads, for distinct hypotheses. The experimental ratio of 71% was most compatible with the assumption that only one dominant telomere, for instance, the shortest, is sufficient for senescence onset.

To conclude, this study supports the following conclusions: (i) telomere length regulation through the protein-counting mechanism has implications for the variability of

the shortest telomere in terms of length, (ii) senescence onset in *S. cerevisiae* is genetically driven and not subject to strong stochastic variations, and (iii) differences in senescence in telomerase-deficient spores from the same tetrad are best explained by the segregation of a single telomere during meiosis. By combining these different lines of evidence, we propose that in *S. cerevisiae* senescence onset is controlled through the shortest telomere.

Acknowledgments

We thank S. Marcand, C. Azzalin, M. G. Ferreira, and Teixeira's lab members for their critical reading of the manuscript and fruitful discussions. Research in Teixeira's laboratory is supported by the European Research Council (ERC-2010-StG 260906—D-END), the Mairie de Paris (Programme Emergences), and Institut Thématique Multi-Organismes (ITMO) Cancer. Research in Holcman's laboratory is supported by an ERC-Starting grant.

Literature Cited

Abdallah, P., P. Luciano, K. W. Runge, M. Lisby, V. Geli *et al.*, 2009 A two-step model for senescence triggered by a single critically short telomere. Nat. Cell Biol. 11: 988–993.

Arkus, N., 2005 A mathematical model of cellular apoptosis and senescence through the dynamics of telomere loss. J. Theor. Biol. 235: 13–32.

Armanios, M., J. K. Alder, E. M. Parry, B. Karim, M. A. Strong *et al.*, 2009 Short telomeres are sufficient to cause the degenerative defects associated with aging. Am. J. Hum. Genet. 85: 823–832.

Blackburn, E. H., 2000 Telomere states and cell fates. Nature 408: 53–56.

Blackburn, E. H., and K. Collins, 2011 Telomerase: an RNP enzyme synthesizes DNA. Cold Spring Harb. Perspect. Biol. 3: a003558.

Brevet, V., A. S. Berthiau, L. Civitelli, P. Donini, V. Schramke *et al.*, 2003 The number of vertebrate repeats can be regulated at yeast telomeres by Rap1-independent mechanisms. EMBO J. 22: 1697–1706.

Britt-Compton, B., R. Capper, J. Rowson, and D. M. Baird, 2009 Short telomeres are preferentially elongated by telomerase in human cells. FEBS Lett. 583: 3076–3080.

Campisi, J., and F. D'adda Di Fagagna, 2007 Cellular senescence: when bad things happen to good cells. Nat. Rev. Mol. Cell Biol. 8: 729–740.

Canela, A., E. Vera, P. Klatt, and M. A. Blasco, 2007 High-throughput telomere length quantification by FISH and its application to human population studies. Proc. Natl. Acad. Sci. USA 104: 5300–5305.

Cech, T. R., 2004 Beginning to understand the end of the chromosome. Cell 116: 273–279.

D'adda Di Fagagna, F., P. M. Reaper, L. Clay-Farrace, H. Fiegler, P. Carr *et al.*, 2003 A DNA damage checkpoint response in telomere-initiated senescence. Nature 426: 194–198.

Enomoto, S., L. Glowczewski, and J. Berman, 2002 MEC3, MEC1, and DDC2 are essential components of a telomere checkpoint pathway required for cell cycle arrest during senescence in *Saccharomyces cerevisiae*. Mol. Biol. Cell 13: 2626–2638.

Griffith, J. D., L. Comeau, S. Rosenfield, R. M. Stansel, A. Bianchi *et al.*, 1999 Mammalian telomeres end in a large duplex loop. Cell 97: 503–514.

Hardy, C. F., L. Sussel, and D. Shore, 1992 A RAP1-interacting protein involved in transcriptional silencing and telomere length regulation. Genes Dev. 6: 801–814.

Hayflick, L., 1965 The limited in vitro lifetime of human diploid cell strains. Exp. Cell Res. 37: 614–636.

Hemann, M. T., M. A. Strong, L. Y. Hao, and C. W. Greider, 2001 The shortest telomere, not average telomere length, is critical for cell viability and chromosome stability. Cell 107: 67–77.

Ijpma, A. S., and C. W. Greider, 2003 Short telomeres induce a DNA damage response in *Saccharomyces cerevisiae*. Mol. Biol. Cell 14: 987–1001.

Jain, D., and J. P. Cooper, 2010 Telomeric strategies: means to an end. Annu. Rev. Genet. 44: 243–269.

Jeyapalan, J. C., and J. M. Sedivy, 2008 Cellular senescence and organismal aging. Mech. Ageing Dev. 129: 467–474.

Kowald, A., 1997 Possible mechanisms for the regulation of telomere length. J. Mol. Biol. 273: 814–825.

Levy, M. Z., R. C. Allsopp, A. B. Futcher, C. W. Greider, and C. B. Harley, 1992 Telomere end-replication problem and cell aging. J. Mol. Biol. 225: 951–960.

Lundblad, V., and J. W. Szostak, 1989 A mutant with a defect in telomere elongation leads to senescence in yeast. Cell 57: 633–643.

Lustig, A. J., S. Kurtz, and D. Shore, 1990 Involvement of the silencer and UAS binding protein RAP1 in regulation of telomere length. Science 250: 549–553.

Marcand, S., E. Gilson, and D. Shore, 1997 A protein-counting mechanism for telomere length regulation in yeast. Science 275: 986–990.

Marcand, S., V. Brevet, and E. Gilson, 1999 Progressive cis-inhibition of telomerase upon telomere elongation. EMBO J. 18: 3509–3519.

Martens, U. M., E. A. Chavez, S. S. Poon, C. Schmoor, and P. M. Lansdorp, 2000 Accumulation of short telomeres in human fibroblasts prior to replicative senescence. Exp. Cell Res. 256: 291–299.

Nugent, C. I., T. R. Hughes, N. F. Lue, and V. Lundblad, 1996 Cdc13p: a single-strand telomeric DNA-binding protein with a dual role in yeast telomere maintenance. Science 274: 249–252.

Op Den Buijs, J., P. P. Van Den Bosch, M. W. Musters, and N. A. Van Riel, 2004 Mathematical modeling confirms the length-dependency of telomere shortening. Mech. Ageing Dev. 125: 437–444.

Passos, J. F., G. Saretzki, S. Ahmed, G. Nelson, T. Richter *et al.*, 2007 Mitochondrial dysfunction accounts for the stochastic heterogeneity in telomere-dependent senescence. PLoS Biol. 5: e110.

Proctor, C. J., and T. B. Kirkwood, 2002 Modelling telomere shortening and the role of oxidative stress. Mech. Ageing Dev. 123: 351–363.

Proctor, C. J., and T. B. Kirkwood, 2003 Modelling cellular senescence as a result of telomere state. Aging Cell 2: 151–157.

Ritchie, K. B., J. C. Mallory, and T. D. Petes, 1999 Interactions of TLC1 (which encodes the RNA subunit of telomerase), TEL1, and MEC1 in regulating telomere length in the yeast *Saccharomyces cerevisiae*. Mol. Cell. Biol. 19: 6065–6075.

Rodriguez-Brenes, I. A., and C. S. Peskin, 2010 Quantitative theory of telomere length regulation and cellular senescence. Proc. Natl. Acad. Sci. USA 107: 5387–5392.

Sahin, E., and R. A. Depinho, 2012 Axis of ageing: telomeres, p53 and mitochondria. Nat. Rev. Mol. Cell Biol. 13: 397–404.

Sahin, E., S. Colla, M. Liesa, J. Moslehi, F. L. Muller *et al.*, 2011 Telomere dysfunction induces metabolic and mitochondrial compromise. Nature 470: 359–365.

Schulz, V. P., and V. A. Zakian, 1994 The Saccharomyces PIF1 DNA helicase inhibits telomere elongation and de novo telomere formation. Cell 76: 145–155.
Singer, M. S., and D. E. Gottschling, 1994 TLC1: template RNA component of *Saccharomyces cerevisiae* telomerase. Science 266: 404–409.
Smith, J. R., and R. G. Whitney, 1980 Intraclonal variation in proliferative potential of human diploid fibroblasts: stochastic mechanism for cellular aging. Science 207: 82–84.
Tan, Z., 1999 Intramitotic and intraclonal variation in proliferative potential of human diploid cells: explained by telomere shortening. J. Theor. Biol. 198: 259–268.
Teixeira, M. T., M. Arneric, P. Sperisen, and J. Lingner, 2004 Telomere length homeostasis is achieved via a switch between telomerase- extendible and -nonextendible states. Cell 117: 323–335.
Van Steensel, B., and T. De Lange, 1997 Control of telomere length by the human telomeric protein TRF1. Nature 385: 740–743.
Walmsley, R. M., and T. D. Petes, 1985 Genetic control of chromosome length in yeast. Proc. Natl. Acad. Sci. USA 82: 506–510.
Wellinger, R. J., and V. A. Zakian, 2012 Everything you ever wanted to know about *Saccharomyces cerevisiae* telomeres: beginning to end. Genetics 191: 1073–1105.
Wotton, D., and D. Shore, 1997 A novel Rap1p-interacting factor, Rif2p, cooperates with Rif1p to regulate telomere length in *Saccharomyces cerevisiae*. Genes Dev. 11: 748–760.
Zou, Y., A. Sfeir, S. M. Gryaznov, J. W. Shay, and W. E. Wright, 2004 Does a sentinel or a subset of short telomeres determine replicative senescence? Mol. Biol. Cell 15: 3709–3718.

Communicating editor: N. Hunter

GENETICS

Supporting Information
http://www.genetics.org/lookup/suppl/doi:10.1534/genetics.113.152322/-/DC1

The Length of the Shortest Telomere as the Major Determinant of the Onset of Replicative Senescence

Zhou Xu, Khanh Dao Duc, David Holcman, and Maria Teresa Teixeira

DOI: 10.1534/genetics.113.152322

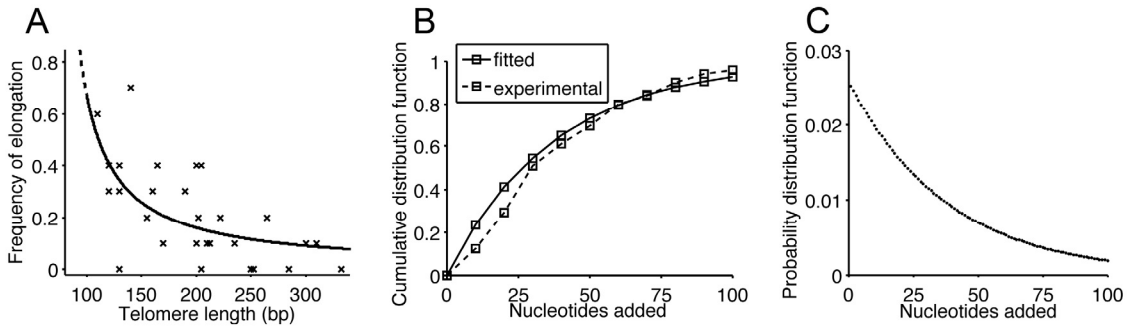

Figure S1 Numerical fit of the parameters using data from (Teixeira *et al.* 2004). *(A)* Numerical fit of the probability of elongation. The probability of elongation (continuous line) from equation 2 was plotted as a function of telomere length for parameters β = 0.048 and L_0 = 90 bp. This function was fitted to the data from (Teixeira *et al.* 2004) (dots). Goodness of fit was given by SSE = 0.6021 (summed square of residuals), R-square = 0.378, adjusted R-square = 0.3558 and RMSE = 0.1466 (root mean squared error). *(B)* Numerical fit of the law of the number of nucleotides b added per elongation. In continuous line, the cumulative distribution function of the geometrical law of parameter p was plotted and fitted to the empirical cumulative distribution extracted from experimental data from Teixeira et al., 2004 (dotted line). We found a value for p = 0.026. Goodness of fit was given by SSE = 0.03822, R-square = 0.9688, adjusted R-square = 0.9688 and RMSE = 0.06182. *(C)* Probability distribution function of b. The probability distribution function associated with the value p = 0.026 found in *(B)* was plotted.

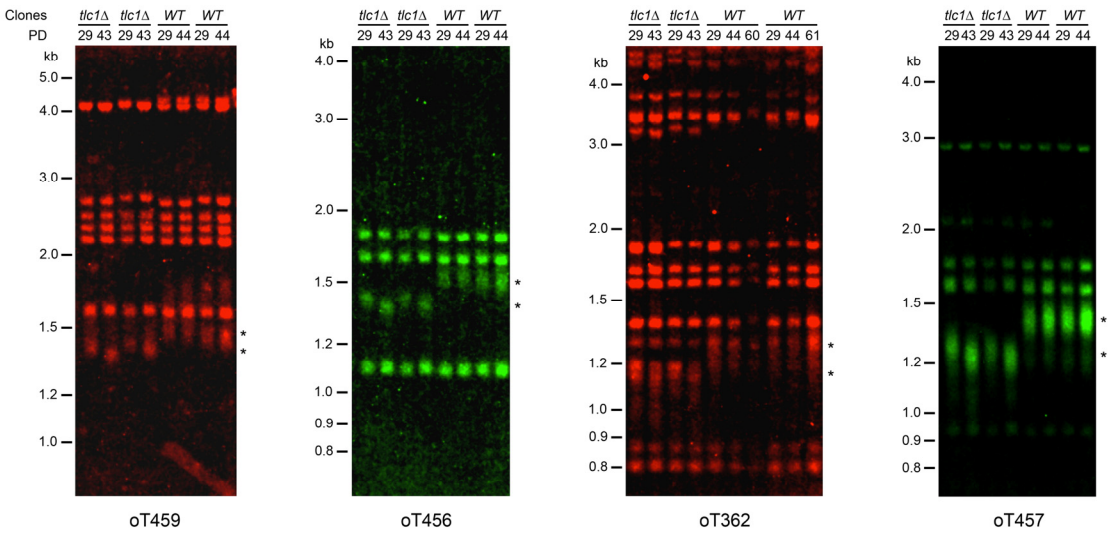

Figure S2 Other examples of single-telomere Southern blots using oT459, oT456, oT362 and oT457 fluorescent probes. Telomerase-positive (wild-type, WT) or negative (*tlc1Δ*) cells from the same tetrad were harvested at different population doublings (PD). Genomic DNAs were extracted, digested with the adequate enzyme (NdeI/BstEII or BstNI) and Southern blots were performed using the indicated probe. Different non specific bands could be observed for each probe. The positions of the telomere signals are marked with the asterisks.

File S1

Supporting Material and Methods

Numerical implementation and parameter estimation.

Numerical simulations and parameter estimation were performed using Matlab (R2012a version). To estimate the values of the parameters β and L_0 in equation 2, we fitted equation 2 to experimental data of (Teixeira *et al.* 2004) (Fig. S1*A*) using the fitting toolbox of Matlab. The parameter p for the elongation length was estimated from the empirical cumulative distribution of the elongation length (Teixeira *et al.* 2004), which we fitted with the cumulative distribution function of parameter p (Fig. S1*B*). The probability function of the increasing length b was plotted in figure S1*C*.

To approximate the probability $P(L)$ of elongation of a telomere of length L, we used the following function

$$P(L)=\frac{1}{1+\beta(L-L_0)}, \quad (*)$$

where β and L_0 are fitting constant parameters. This expression was inferred from the biochemical process in which telomerase and Rap1/Rif1/Rif2 compete for the same substrate, namely the telomere (Fig. 1*A*).

To obtain the equation (*), we shall now derive from the analysis of chemical reactions regulating telomere length expression. There are two opposite reactions:

First, when telomerase is recruited, the telomere elongates:

$$Telomere + Telomerase \xrightarrow{k_2} Elongated\ Telomere \qquad (3)$$

where k_2 is the rate constant of the reaction.

Conversely, a shortening event occurs if the amount of Rap1/Rif1/Rif2 in *cis* is enough to inhibit telomerase recruitment:

$$Telomere + Rap1/Rif1/Rif2 \xrightarrow{k_1(L_n-L_0)} Shortened\ Telomere \qquad (4)$$

where $k_1(L_n-L_0)$ is the rate constant of the reaction.

We consider that the number of telomere-bound Rap1/Rif1/Rif2 protein complexes is proportional to the telomere length (Marcand *et al.* 1997) and thus the rate constant in equation 4 is proportional to the telomere length L_n-L_0. Combining equations 3 and 4, we obtain the steady-state probability distribution $P(L_n)=\frac{1}{1+\beta(L_n-L_0)}$ used in equation 2, where $\beta=\frac{k_1}{k_2}$. We fitted this expression to experimental data, and we found $\beta=0.045$ and $L_0=90$ bp (Fig. S1*A* and Table 1).

In the present model, we consider that the correspondence between the amount of Rap1/Rif1/Rif2 protein complexes and the constant rate of equation 4 is linear over the entire range of telomere lengths used for our simulations. Indeed, this assumption is verified *a posteriori* since expression (*) was a good fit to the data on the entire length interval.

Statistical analysis.

All statistical analyses were performed using the statistical toolbox of Matlab. The means of senescence indices measured by the spot assay were tested for statistical difference by unpaired two-sample Student's *t*-test, with "the means of senescence indices are equal for the two considered sets" being the null hypothesis. The ratio of the number of tetrads with differential senescence between two *tlc1Δ* spores to the total number of tetrads was compared to theoretical ratios using Pearson's χ^2 goodness-of-fit test, which is commonly used to assess whether an observed distribution differs from a theoretical one, with "the observed ratio is equal to the theoretical one" being the null hypothesis. We also used Pearson's χ^2 goodness-of-fit test to compare simulated distributions to the experimental one (Fig. 1*F*), with "the frequency distribution of telomere lengths in the same in the simulation and the experiment" as the null hypothesis. For both statistical tests, we used the *p*-value to evaluate the probability of obtaining the test statistic assuming the null hypothesis. 0.05 was chosen as a threshold for the *p*-value, below which we rejected the null hypothesis.

Oligonucleotide probe design.

The probes used for single-telomere Southern blot were designed using the sequence of the S288C strain from Saccharomyces Genome Database (SGD) version R64-1-1 and information about W303 strain telomeres from Ed Louis's group's website (http://www.nottingham.ac.uk/biology/people/louis/telomere-data-sets.aspx). All analyses were performed using Geneious Pro 5.5.2. To design specific probes, we tested divergent regions among telomeres within 1.5 kb of the telomeric repeats. Each candidate was blasted against the whole genome using the blastn algorithm and selected for its specificity, although cross-reactivity with nonterminal restriction region was allowed. To confirm specificity, we used each probe as a primer to amplify the corresponding telomeric region by PCR, with another specifically designed primer located at the junction of the telomeric repeats and the specific subtelomeric region. We only used probes for which PCR amplified a unique band. The PCR product was then sequenced (Eurofins MWG Operon), and the sequence was compared to the S288C genome. With the exception of the XIV-R telomere (Table S1), which failed to be sequenced, all sequences either were completely identical to S288C sequences or displayed some point mutations (only for the XI-L telomere), which was expected since the yT337 background is different from S288C. As IX-L and X-L subtelomeres were identical, the oT457 probe was not specific to a unique telomere (Table S1).

Quantitative senescence assay.

The quantitative senescence assay used in this study was based on the semi-quantitative senescence assay described in (Abdallah *et al.* 2009). In most experiments, yT337 tetrads were dissected and spores were grown for 2 days at 30°C on a YPD plate. A third of each colony was resuspended in 5 µl water, boiled at 95°C for 5 min, and used as a substrate in PCR for genotyping *TLC1* locus. Colonies grown from single spores were resuspended in water in microtiter plates, and their concentrations were normalized at 800,000 cells per ml after OD (optical density) at 600 nm using an Epoch spectrophotometer (Biotek). For each cell suspension, eight replicates of 10-fold serial dilution spots were grown on a YPD plate, so as to assess the intraclonal variation that could arise and to statistically compare cell growth from different spores. The spots were grown for 2 days at 30°C. For each replicate, the most concentrated spot was then resuspended, normalized at 800,000 cells per ml, and re-spotted with serial dilutions. The same procedure was repeated for the next passage as well. Compared to the quantification procedure in (Abdallah *et al.* 2009), a new senescence index was used in this study. After 2 days of growth, spot plates were scanned at 1200 dpi using an Epson Perfection V750 Pro scanner. Images were processed with ImageJ. After background subtraction, all the spot intensities were measured and plotted against the logarithm of the 10-fold dilutions. The senescence index corresponded to the logarithm of the 10-fold dilution needed to grow the cells up to a set standard intensity value, which corresponded to the median intensity reached by wild-type telomerase-positive cells in 2 days of growth. For example, an index value of 1.3 for a given spore at passage 2 meant that, at passage 2, these cells would have needed to be diluted to $10^{-1.3}$ (starting with 800,000 cells per ml concentration) in order to reach, after 2 days, the set standard intensity value.

File S2

Supporting Text

Calculation of the ratio of tetrads displaying different senescence for their telomerase-deficient spores to the total number of tetrads.

We made the assumption that telomeres are independently regulated regarding their length, as suggested in figure 1*D* where two telomeres in different clones did not show correlated lengths and in (Shampay and Blackburn 1988). We considered a *TLC1/tlc1Δ* diploid cell with 64 independent telomeres. Let us order these 64 telomeres by their length: $L_1 \leq L_2 \leq \ldots \leq L_{64}$, corresponding to the telomeres T_1, T_2, …, T_{64}, respectively. At prophase I of meiosis, all 64 telomeres are replicated. For a given telomere T_n ($1 \leq n \leq 64$), we assumed that the length of the two replicated strands was the same: if we called the two telomeres T_n and T_n', we assumed that $L_n = L_n'$ ($1 \leq n \leq 64$). In theory, there should be a difference of about the overhang length (~10 nt) between L_n and L_n'. As shown in figure 5*A*, however, this difference has no phenotypic consequence in the senescence onset, as mother and daughter cells always displayed similar senescence, even though mitotic replication should generate the same difference in length for a given telomere. Therefore, this assumption seems valid considering the sensitivity of the spot assay.

Meiotic crossing-overs would exchange telomeres between homologous chromosomes with the highest ratio as telomeres are located at the ends of chromosomes. Thus, meiosis randomly divides out these 128 telomeres (T_1, T_1', T_2, T_2', …, T_{64}, T_{64}') between the four spores.

First hypothesis: the senescence signal is controlled by a dominant telomere, likely the shortest.

Let us analyze how telomeres T_1 and T_1' segregate between the four spores. There are 12 possibilities (see below for the complete list). In two cases, both T_1 and T_1' fall into the two *tlc1Δ* spores (either T_1 into spore 1 and T_1' into spore 2, or the reverse). Thus, there is a 1/6 probability that T_1 and T_1' fall into the two *tlc1Δ* spores. Similarly, there is also a 1/6 probability that T_1 and T_1' fall into the two *TLC1* spores. That leaves a 2/3 probability that T_1 falls into a *tlc1Δ* spore and T_1' falls into a *TLC1* spore, or the reverse[*].

Under the hypothesis that a dominant telomere, likely the shortest shortest controls the senescence signal, there should be, for the two *tlc1Δ* spores:

1- No difference in senescence if both T_1 and T_1' fall into the two *tlc1Δ* spores (P = 1/6)

[*] The same result could be obtained by classical tetrad analysis where 1/6 are ditype parental (for instance, T_1 and T_1' in the two *tlc1Δ*), 1/6 ditype non-parental (T_1 and T_1' in the two *TLC1*) and 2/3 are tetratypes.

2- Differential senescence if either T_1 or T_1' falls into a *tlc1Δ* spore but not the other (P = 2/3)

3- Unknown result if both T_1 and T_1' fall into the two *TLC1* spores (P = 1/6), because senescence onset should then be controlled by T_2 and T_2'. We can then apply the same reasoning to T_2 and T_2' and show that with a 1/6 probability, the two *tlc1Δ* spores should display the same senescence onset; with a 2/3 probability, different senescence onsets; and with a 1/6 probability, a result that would depend on T_3 and T_3'.

Therefore, we recursively show that the two *tlc1Δ* spores should have the same senescence onset with the following probability:

$$P = 1/6 + (1/6)^2 + \ldots + (1/6)^{32} \approx 1/5 = 20\%$$

And the two *tlc1Δ* spores should display differential senescence with the complementary probability:

$$1 - P \approx 80\%$$

Second hypothesis: the senescent cell is not able to detect the shortest telomere.

In this case, a minimal postulate would be that the senescent cell cannot distinguish between the shortest and the second shortest telomeres, which is equivalent, for calculation simplicity, to $L_1 = L_2$ while keeping control by the shortest telomere as an assumption. Other postulates would lead to an even lower probability of different senescence onsets for the two *tlc1Δ* spores. This case is best illustrated by a two-way table with all 12 possible segregations of T_1/T_1' into the four spores along one dimension and all 12 possible segregations of T_2/T_2' on the other. The output in each square will be "=", meaning "same senescence onset for the two *tlc1Δ* spores", if the two *tlc1Δ* spores have either one of the four T_1, T_1', T_2, or T_2'; "≠", meaning "different senescence onsets for the two *tlc1Δ* spores", if one has T_1, T_1', T_2, or T_2' but the other none of these telomeres; or "?" if these four telomeres fall into the two *TLC1* spores.

The 12 possibilities for segregation are listed below:

	*tlc1*Δ #1	*tlc1*Δ #2	*TLC1* #1	*TLC1* #2
1	T	T'		
2	T'	T		
3	T		T'	
4	T			T'
5		T	T'	
6		T		T'
7	T'		T	
8	T'			T
9		T'	T	
10		T'		T
11			T	T'
12			T'	T

The rules we stated above lead to the following two-way table:

$T_2 \backslash T_1$	1	2	3	4	5	6	7	8	9	10	11	12
1	=	=	=	=	=	=	=	=	=	=	=	=
2	=	=	=	=	=	=	=	=	=	=	=	=
3	=	=	≠	≠	=	=	≠	≠	=	=	≠	≠
4	=	=	≠	≠	=	=	≠	≠	=	=	≠	≠
5	=	=	=	=	≠	≠	=	=	≠	≠	≠	≠
6	=	=	=	=	≠	≠	=	=	≠	≠	≠	≠
7	=	=	≠	≠	=	=	≠	≠	=	=	≠	≠
8	=	=	≠	≠	=	=	≠	≠	=	=	≠	≠
9	=	=	=	=	≠	≠	=	=	≠	≠	≠	≠
10	=	=	=	=	≠	≠	=	=	≠	≠	≠	≠
11	=	=	≠	≠	≠	≠	≠	≠	≠	≠	?	?
12	=	=	≠	≠	≠	≠	≠	≠	≠	≠	?	?

In these 144 squares, if we neglect the four "?" squares, we obtain the following probability of getting two *tlc1Δ* spores with the same senescence onset:

$$P \approx 76/140 \approx 54\%$$

And the probability for the two *tlc1Δ* spores to display different senescence onset would be:

$$1 - P \approx 46\%$$

We can notice that this calculation is also valid if the phenotypic assay, namely the spot assay, is not sensitive enough to distinguish between senescence onsets induced by the difference in length between T_1 and T_2. This might explain why there was a slight difference between our experimental 71% ratio and the theoretical 80% ratio.

Lastly, we also considered the uninvestigated possibility that telomerase may act at prophase I of meiosis before division on T_1 but not T_1' (or the reverse). Given the range of length of T_1 and T_1' in our simulations (around 180–200 bp), the probability of extension by telomerase is around 15% (Fig. S1*A*). This would generate a difference in length between T_1 and T_1' if telomerase acts on one but not the other, which corresponds to a probability of 0.15 × (1-0.15) = 0.1275. This has to be applied to all cases where we are supposed to observe a similar senescence for the two telomerase-deficient spores because they received T_1 and T_1'. Such cases amount to 2 out of the 12 possibilities in the previous table. Thus, these 2/12 ≈ 17% have to be corrected down by the 0.1275 probability of extension, which leads to 0.1275 × 2/12 ≈ 0.02. Overall, if we consider that telomerase can differentially act at prophase I on two sister chromatid telomeres, this would theoretically change the ratio of tetrads with similar senescence for the two telomerase-deficient spores from 20% to ~18%, and the ratio of tetrads with different senescence onsets for the two telomerase-deficient spores from 80% to ~82%.

SI REFERENCE

Shampay, J., and E. H. Blackburn, 1988 Generation of telomere-length heterogeneity in Saccharomyces cerevisiae. Proc Natl Acad Sci U S A 85**:** 534-538.

Table S1 Oligonucleotides probes used in single-telomere Southern blot.

Probe name	Telomere	Subtelomere elements	Restriction enzyme	Probe sequence	Size of terminal restriction fragment in bp	Quality[1]
oT355	I-L	X	NdeI	GCTTGTGGTAGCAACACTATCATGGTATCAC	965	+++
oT356	II-R	X	BstEII	CTAACACAATCCTAACAGTACCCTATTCTAACCCTGATG	1308	++
oT357	III-L	X	BstEII	CTCAATTTATACACACTTATGTCAATATAACCACAAAATCAC	828	+
oT358	XI-L	X	BstEII	TTTTACCTGTCTCCAAACCTACCCTCACATTACCCTA	964	+
oT360	VI-R	X	NdeI	CATTCCGAACGCTATTCCAGAAAGTAGTCCAGCC	688	+++
oT361	VII-L	X	BstEII	CTATTTTCTTGAACGGATGACATTTCATGTTG	840	++
oT362	XIV-R	X	NdeI	TTCTACAACTCCAACCACCATCCATCTCTCTACTTACCACTA	988	+
oT455	X-R	X	NdeI	CATGCCATACTCACTTGCACTTGTATACTGATATGG	391	+
oT456	I-R	X	BstNI	CAAGATGGTAAAAGATTGAAGGCGTATCGTGGTATGG	1171	+++
oT457	IX-L/X-L	XY'/XY'	BstNI	GTTGTTGTGGAAGCGCTCGAGAAAGG	1165	+++
oT459	XV-L	X	BstNI	GTGGTATTGATACGTAATTGAGTG	1149	+++

[1]Refers to the sensitivity and the specificity of the oligonucleotide probe:

+++ sensitive and specific telomeric signal; ++ less sensitive but specific telomeric signal; + presence of non specific bands that may hinder analysis